Submitted to the
XXII International Symposium on Lepton-Photon Interactions at High Energy
30 June - 5 July, Uppsala, Sweden

Abstract: 255 **Session: EW&B**

Measurement of high-Q^2 deep inelastic scattering cross sections with longitudinally polarised electron beams at HERA

ZEUS Collaboration

Abstract

Measurements of the cross sections for neutral and charged current deep inelastic scattering in e^-p collisions with longitudinally polarised electron beams are presented. The total cross section for e^-p charged current deep inelastic scattering is presented at positive and negative values of electron beam longitudinal polarisation. In addition, single differential cross sections are presented for charged and neutral current deep inelastic scattering in the kinematic region $Q^2 > 200\,\mathrm{GeV}^2$. The measurements are based on data samples of integrated luminosities of $41.7\,\mathrm{pb}^{-1}$ and $53.5\,\mathrm{pb}^{-1}$ for charged and neutral current, respectively, collected with the ZEUS detector at HERA in 2004 and 2005 at a centre-of-mass energy of 318 GeV. The measured cross sections are compared with the predictions of the Standard Model.

1 Introduction

Deep inelastic scattering (DIS) of leptons off nucleons has proved to be a key tool in the understanding of the structure of the proton and the form of the Standard Model (SM). The HERA *ep* collider has made possible the exploration of DIS at high values of negative four-momentum-transfer squared, Q^2. Using data taken in the years 1994-2000 the H1 and ZEUS collaborations have reported measurements of the cross sections for charged current (CC) and neutral current (NC) DIS [1–18]. These measurements extend the kinematic region covered by fixed-target proton structure measurements [19–25] to higher Q^2 and allow the HERA experiments to probe the electroweak sector of the Standard Model.

The Standard Model predicts that the cross sections for charged and neutral current *ep* DIS should exhibit dependence on the longitudinal polarisation of the incoming lepton beam. In the charged current case the dependence is predicted to be linear with the cross section becoming zero for right-handed (left-handed) electron (positron) beams, due to the chiral nature of the Standard Model.

This paper presents measurements of the cross sections for e^-p CC and NC DIS with longitudinally polarised electron beams. The measurements are based on data samples of integrated luminosities of $6.5\,\text{pb}^{-1}$ and $8.4\,\text{pb}^{-1}$ for charged and neutral current, respectively, collected at a mean luminosity weighted polarisation of 29.2% , and luminosities of $35.3\,\text{pb}^{-1}$ and $45.1\,\text{pb}^{-1}$ for charged and neutral current, respectively, collected at a polarisation of -25.9% with the ZEUS detector in 2004 and 2005. During this time HERA collided protons of energy 920 GeV with electrons of energy 27.5 GeV, yielding collisions at a centre-of-mass energy of 318 GeV. The measured cross sections are compared to the Standard Model predictions and previous ZEUS measurements in positron-proton scattering with longitudinally polarised positron beams [26].

2 Kinematic variables and cross sections

Inclusive deep inelastic lepton-proton scattering can be described in terms of the kinematic variables x, y and Q^2. The variable Q^2 is defined to be $Q^2 = -q^2 = -(k - k')^2$ where k and k' are the four-momenta of the incoming and scattered lepton, respectively. Bjorken x is defined by $x = Q^2/2P \cdot q$ where P is the four-momentum of the incoming proton. The variable y is defined by $y = P \cdot q/P \cdot k$. The variables x, y and Q^2 are related by $Q^2 = sxy$, where $s = 4E_eE_p$ is the square of the lepton-proton centre-of-mass energy (neglecting the masses of the incoming particles).

The electroweak Born level cross section for the CC reaction, $e^-p \rightarrow \nu_e X$, with a longitudinally polarised electron beam (defined in Eqn. (1)), can be expressed as [27]

$$\frac{d^2\sigma^{\rm CC}(e^-p)}{dxdQ^2} = (1-\mathcal{P})\frac{G_F^2}{4\pi x}\left(\frac{M_W^2}{M_W^2+Q^2}\right)^2\left[Y_+F_2^{\rm CC}(x,Q^2)+Y_-xF_3^{\rm CC}(x,Q^2)-y^2F_L^{\rm CC}(x,Q^2)\right],$$

where G_F is the Fermi constant, M_W is the mass of the W boson and $Y_\pm = 1 \pm (1-y)^2$. The structure functions $F_2^{\rm CC}$ and $xF_3^{\rm CC}$ contain sums and differences of the quark and anti-quark parton density functions (PDFs) and $F_L^{\rm CC}$ is the longitudinal structure function. The longitudinal polarisation of the electron beam is defined as

$$\mathcal{P} = \frac{N_R - N_L}{N_R + N_L}, \tag{1}$$

where N_R and N_L are the numbers of right and left-handed electrons in the beam. Similarly the cross section for the NC reaction, $e^-p \to e^-X$, can be expressed as

$$\frac{d^2\sigma^{\rm NC}(e^-p)}{dxdQ^2} = \frac{2\pi\alpha^2}{xQ^4}[H_0^- + \mathcal{P}H_{\mathcal{P}}^-],$$

where α is the QED coupling constant and H_0^- and $H_{\mathcal{P}}^-$ contain the unpolarised and polarised structure functions, respectively.

ZEUS is a multipurpose detector described in detail elsewhere [28]. Charged current events are characterised by a large missing transverse momentum, $P_{T,\rm miss}$, which is calculated as

$$P_{T,\rm miss}^2 = P_x^2 + P_y^2 = \left(\sum_i E_i \sin\theta_i \cos\phi_i\right)^2 + \left(\sum_i E_i \sin\theta_i \sin\phi_i\right)^2,$$

where the sum runs over all calorimeter energy deposits E_i, and θ_i and ϕ_i are the polar and azimuthal angles of the energy deposits as viewed from the interaction vertex. The hadronic polar angle, γ_h, is defined by $\cos\gamma_h = (P_{T,\rm miss}^2 - \delta^2)/(P_{T,\rm miss}^2 + \delta^2)$, where $\delta = \sum(E_i - E_i\cos\theta_i) = \sum(E - P_z)_i$. In the naive Quark Parton Model, γ_h gives the scattering angle of the struck quark in the lab frame. The total transverse energy, E_T, is given by $E_T = \sum E_i \sin\theta_i$.

Neutral current events are characterised by the presence of a high-energy isolated scattered electron in the detector. It follows from longitudinal momentum conservation that for well measured NC events δ peaks at twice the electron beam energy, i.e. 55 GeV.

The kinematic variables for charged current events were reconstructed from the measured $P_{T,\rm miss}$ and δ using the Jacquet-Blondel method [29]. The double-angle method [30] was used for the neutral current events to estimate the kinematic variables from the polar angles of the scattered electron and the hadronic final state.

In the following, measurements of total cross sections and differential cross sections in x, y and Q^2 for the charged current reaction are presented. In addition, differential cross sections in Q^2 were measured for the neutral current reaction.

3 Monte Carlo simulation

Monte Carlo simulation (MC) was used to determine the efficiency for selecting events, the accuracy of kinematic reconstruction, to estimate the background rate and to deduce cross sections for the full kinematic region from the data. A sufficient number of events were generated to ensure that uncertainties from MC statistics were small. The MC samples were normalised to the total integrated luminosity of the data.

Neutral and charged current DIS events including radiative effects were simulated using the DJANGOH 1.3 [31] generator. The hadronic final state was simulated using the colour-dipole model of ARIADNE 4.10 [32] and, as a systematic check, the MEPS model of LEPTO 6.5 [33]. Both programs use the Lund string model of JETSET 7.4 [34] for the hadronisation. Photoproduction background in the charged current sample was estimated using events simulated with HERWIG 5.9 [35].

4 Event selection

4.1 Charged current

The following criteria were imposed to select charged current events and reject background.

- missing transverse momentum: $P_{T,\mathrm{miss}} > 12\,\mathrm{GeV}$ was required and, in addition, the missing transverse momentum, excluding the calorimeter cells adjacent to the forward beam hole, $P'_{T,\mathrm{miss}}$, was required to exceed $10\,\mathrm{GeV}$;
- primary vertex: events were required to satisfy $|Z_{\mathrm{vtx}}| < 50$ cm. The Z coordinate of the ep interaction vertex, reconstructed using tracks in the central tracking detectors, was required to be in the centre of the detector. For events with an hadronic angle, γ_h, of less than 23° the vertex position was set to the nominal value of zero, and the $P_{T,\mathrm{miss}}$ and $P'_{T,\mathrm{miss}}$ thresholds increased to 14 and 12 GeV, respectively;
- rejection of photoproduction: $P_{T,\mathrm{miss}}/E_T > 0.5$ was required. This requirement demanded an azimuthally collimated energy flow. In addition, it was required that the angle between the missing transverse momentum measured by the tracks and that

measured by the calorimeter was less than one radian for events with $P_{T,\mathrm{miss}} > 30\,\mathrm{GeV}$. This requirement was tightened to 0.5 radians for events with $P_{T,\mathrm{miss}} < 30\,\mathrm{GeV}$;

- rejection of NC DIS: NC DIS events with a poorly measured scattered electron or hadronic jet can have significant missing transverse momentum. Events with $\delta > 30\,\mathrm{GeV}$ and an isolated electromagnetic cluster in the calorimeter were rejected;
- rejection of non-*ep* background: interactions between the beams and residual gas in the beam pipe or upstream accelerator components can lead to events with significant missing transverse momentum, however for these interactions the arrival times of energy deposits in the calorimeter are inconsistent with the bunch crossing time. The arrival times were used to reject such events. Muon finding algorithms based on tracking, calorimeter and muon chamber information were used to reject events caused by cosmic rays or muons in the beam halo. In addition, the shape of hadronic showers in the calorimeter was used to reject halo muon events depositing energy in the forward calorimeter;
- kinematic region: events were required to satisfy $Q^2_{\mathrm{JB}} > 200\,\mathrm{GeV}^2$ and $y_{\mathrm{JB}} < 0.9$, where Q^2_{JB} and y_{JB} are the Jaquet-Blondel estimators of Q^2 and y, respectively. These requirements restricted the event sample to a kinematic region where the resolution of the kinematic quantities is good and the background is small.

A total of 2323 candidate events passed the selection criteria. The background contamination was estimated to be typically less than 1% but was as high as 15% in the lowest Q^2 bin of the positive polarisation sample. Figures 1 and 2 show comparisons of data and MC distributions for the negative polarisation and positive polarisation CC samples, respectively. The Monte Carlo gives a good description of the data.

4.2 Neutral current

The following criteria were imposed to select neutral current events.

- electron identification: an algorithm which combined information from the energy deposits in the calorimeter with tracks measured in the central tracking detector (CTD) was used to identify scattered electrons. A fiducial-volume cut was applied to guarantee that the experimental acceptance was well understood. To ensure high purity and reject background, the identified electron was required to have an energy of at least $10\,\mathrm{GeV}$ and be isolated such that the energy in an $\eta - \phi$ cone of radius 0.8 centred on the electron, not associated with the electron, was less than $5\,\mathrm{GeV}$. For events in which an electron was found within the acceptance of the CTD a track matched to the energy deposit in the calorimeter was required. For events with an electron at a smaller polar angle with respect to the proton beam direction than the acceptance of the CTD, the track requirement was replaced with the requirement that the transverse momentum of the electron exceeded 30 GeV;

- primary vertex: events were required to satisfy $|Z_{\rm vtx}| < 50$ cm. The Z coordinate of the ep interaction vertex, reconstructed using tracks in the central tracking detector, was required to be in the centre of the detector;
- background rejection: the requirement $38 < \delta < 65$ GeV was imposed to remove photoproduction and beam-gas events, and to reduce the number of events with significant QED initial state radiation. To further reduce background from photoproduction events, y calculated from the electron method (y_e) was required to satisfy $y_e < 0.95$. The net transverse momentum is expected to be small, so in order to remove cosmic-ray events and beam related background events the quantity $P_T/\sqrt{E_T}$ was required to be less than $4\sqrt{\rm GeV}$, and the quantity P_T/E_T was required to be less than 0.7;
- QEDC rejection: to reduce the size of the QED radiative corrections, elastic Compton scattering events were rejected;
- kinematic region: to avoid regions of phase space in which the MC generator is not valid the quantity $y_{\rm JB}(1-x_{\rm DA})$, where $x_{\rm DA}$ is the double-angle estimator of x, was required to be greater than 0.004. In addition the final event sample was defined by requiring Q^2 calculated from the double-angle method, $Q^2_{\rm DA}$, to satisfy $Q^2_{\rm DA} > 200\,{\rm GeV}^2$.

A total of 95010 candidate events passed the selection criteria. The background contamination is expected to be less than 1% [26]. Figure 3 shows a comparison of data and MC expectation distributions for the NC sample. The Monte Carlo gives a generally good description of the data.

5 Systematic uncertainties

The major sources of systematic uncertainty in the CC cross sections were the calorimeter energy scale and the uncertainty in the parton-shower scheme. The former was estimated by varying the energy scale of the whole calorimeter by ± 2%. The resulting shifts in the cross sections were typically less than 10%, but increased to $30-40\%$ in the highest Q^2 bins and 20% in the highest x bin. To estimate the sensitivity of the results to the details of the simulation of the hadronic final state, the LEPTO MEPS model was used instead of the ARIADNE model for calculating the acceptance corrections. The largest effects of $\sim 10\%$ were observed at low Q^2 and low x. The systematic effects of the selection cuts were estimated by varying the threshold value of each selection cut independently by around 10%, which is a reasonable match to the resolution. The resulting shifts in the cross sections were typically within ±5%.

The major source of systematic uncertainty in the NC cross section was the uncertainty in the parton-shower scheme which gave changes in the cross section of 2-3%. Uncertainty in the electromagnetic energy scale was estimated by varying the energy scale by $\pm 3\%$, however, due to the use of the double-angle reconstruction, the resulting shifts in the cross section were $0.5-1\%$. The systematic effects of the selection cuts were estimated by varying the threshold value of each selection cut independently by typically 10%, which is a reasonable match to the resolution. The resulting shifts in the cross sections were typically within $\pm 2\%$.

The individual uncertainties were added in quadrature separately for the positive and negative deviations from the nominal cross section values to obtain the total systematic uncertainty. The electron beam polarisation was measured using the HERA Compton polarimeters [36, 37]. The relative uncertainty in the measured polarisation was 1.6% using the longitudinal polarimeter and 3.5% using the transverse polarimeter. The relative uncertainty in the measured luminosity was 5%. The uncertainties in the luminosity and polarisation measurements were not included in the total systematic uncertainty.

6 Results

The total cross section for e^-p CC DIS in the kinematic region $Q^2 > 200\,\mathrm{GeV}^2$ was measured to be

$$\sigma^{\mathrm{CC}}(\mathcal{P} = 0.292 \pm 0.005) = 54.6 \pm 3.5(\mathrm{stat.})^{+1.4}_{-1.1}(\mathrm{syst.})\ \mathrm{pb},$$

and

$$\sigma^{\mathrm{CC}}(\mathcal{P} = -0.259 \pm 0.005) = 86.2 \pm 1.9(\mathrm{stat.})^{+2.6}_{-2.2}(\mathrm{syst.})\ \mathrm{pb}.$$

The total cross section is shown as a function of the longitudinal polarisation of the electron beam in Fig. 4 including the unpolarised ZEUS measurement from the 1998-1999 data [15]. The data are compared to the Standard Model prediction evaluated using the ZEUS-S PDFs [38]. The SM prediction describes the data well. Figure 5 shows the total cross section as a function of polarisation compared to the previous ZEUS measurement in e^+p scattering [26].

The single-differential cross-sections, $d\sigma/dQ^2$, $d\sigma/dx$ and $d\sigma/dy$ for charged current DIS are shown in Fig. 6. A clear difference is observed between the measurements for positive and negative longitudinal polarisation, which is well described by the Standard Model evaluated using the ZEUS-S PDFs.

Figure 7 shows the cross-section $d\sigma/dQ^2$ for NC DIS for positive and negative longitudinal polarisations and the ratio of the two cross sections. Only statistical uncertainties were considered when taking the ratio of the positively and negatively polarised cross sections. The measurements are well described by the SM evaluated using the ZEUS-S PDFs and consistent with the expectations of the electroweak Standard Model for polarised NC DIS, although the statistical precision of the current data set does not allow the polarised effect to be conclusively observed.

7 Summary

The cross sections for neutral and charged current deep inelastic scattering in e^-p collisions with longitudinally polarised electron beams have been measured. The measurements are based on data of integrated luminosities of $41.7\,\text{pb}^{-1}$ and $53.5\,\text{pb}^{-1}$ for charged and neutral current, respectively, collected with the ZEUS detector in 2004 and 2005 at a centre-of-mass energy of 318 GeV. The total cross section for e^-p charged current deep inelastic scattering is presented at positive and negative values of electron beam longitudinal polarisation. In addition, single differential cross sections are presented for charged and neutral current deep inelastic scattering in the kinematic region $Q^2 > 200\,\text{GeV}^2$. The measured cross sections are well described by the predictions of the Standard Model.

References

[1] H1 Coll., T. Ahmed et al., Phys. Lett. **B 324**, 241 (1994).

[2] H1 Coll., S. Aid et al., Z. Phys. **C 67**, 565 (1995).

[3] H1 Coll., S. Aid et al., Phys. Lett. **B 379**, 319 (1996).

[4] H1 Coll., S. Aid et al., Nucl. Phys. **B 470**, 3 (1996).

[5] H1 Coll., C. Adloff et al., Nucl. Phys. **B 497**, 3 (1997).

[6] H1 Coll., C. Adloff et al., Eur. Phys. J. **C 13**, 609 (2000).

[7] H1 Coll., C. Adloff et al., Eur. Phys. J. **C 19**, 269 (2001).

[8] H1 Coll., C. Adloff et al., Eur. Phys. J. **C 21**, 33 (2001).

[9] H1 Coll., C. Adloff et al., Eur. Phys. J. **C 30**, 1 (2003).

[10] ZEUS Coll., M. Derrick et al., Phys. Rev. Lett. **75**, 1006 (1995).

[11] ZEUS Coll., M. Derrick et al., Z. Phys. **C 72**, 47 (1996).

[12] ZEUS Coll., J. Breitweg et al., Eur. Phys. J. **C 11**, 427 (1999).

[13] ZEUS Coll., J. Breitweg et al., Eur. Phys. J. **C 12**, 411 (2000). Erratum in Eur. Phys. J. **C 27**, 305 (2003).

[14] ZEUS Coll., S. Chekanov et al., Eur. Phys. J. **C 21**, 443 (2001).

[15] ZEUS Coll., S. Chekanov et al., Phys. Lett. **B 539**, 197 (2002). Erratum in Phys. Lett. **B 552**, 308 (2003).

[16] ZEUS Coll., S. Chekanov et al., Eur. Phys. J. **C 28**, 175 (2003).

[17] ZEUS Coll., S. Chekanov et al., Eur. Phys. J. **C 32**, 1 (2003).

[18] ZEUS Coll., S. Chekanov et al., Phys. Rev. **D 70**, 052001 (2004).

[19] CDHS Coll., H. Abramowicz et al., Z. Phys. **C 25**, 29 (1984).

[20] CDHSW Coll., J.P. Berge et al., Z. Phys. **C 49**, 187 (1991).

[21] CCFR Coll., E. Oltman et al., Z. Phys. **C 53**, 51 (1992).

[22] BEBC Coll., G.T. Jones et al., Z. Phys. **C 62**, 575 (1994).

[23] NMC Coll., M. Arneodo et al., Nucl. Phys. **B 483**, 3 (1997).

[24] BCDMS Coll., A.C. Benvenuti et al., Phys. Lett. **B 223**, 485 (1989).

[25] E665 Coll., M.R. Adams et al., Phys. Rev. **D 54**, 3006 (1996).

[26] ZEUS Coll., *Charged and neutral current deep inelastic scattering with longitudinally polarised positron beams.* Abstract 254, *XXII International Symposium on Lepton-Photon Interactions at High Energy*, 30 June - 5 July, 2005.

[27] R.J. Cashmore et al., *Proc. the Workshop on Future Physics at HERA*, G. Ingelman, A. De Roeck and R. Klanner (eds.), Vol. 1, p. 163. DESY, Hamburg, Germany (1996).

[28] ZEUS Coll., U. Holm (ed.), *The ZEUS Detector*. Status Report (unpublished), DESY (1993), available on `http://www-zeus.desy.de/bluebook/bluebook.html`.

[29] F. Jacquet and A. Blondel, *Proceedings of the Study for an ep Facility for Europe*, U. Amaldi (ed.), p. 391. Hamburg, Germany (1979). Also in preprint DESY 79/48.

[30] S. Bentvelsen, J. Engelen and P. Kooijman, *Proc. Workshop on Physics at HERA*, W. Buchmüller and G. Ingelman (eds.), Vol. 1, p. 23. Hamburg, Germany, DESY (1992);
K.C. Höger, *Proc. Workshop on Physics at HERA*, W. Buchmüller and G. Ingelman (eds.), Vol. 1, p. 43. Hamburg, Germany, DESY (1992).

[31] G.A. Schuler and H. Spiesberger, *Proc. Workshop on Physics at HERA*, W. Buchmüller and G. Ingelman (eds.), Vol. 3, p. 1419. Hamburg, Germany, DESY (1991);
H. Spiesberger, HERACLES *and* DJANGOH*: Event Generation for ep Interactions at HERA Including Radiative Processes*, 1998, available on `http://www.desy.de/~hspiesb/djangoh.html`.

[32] L. Lönnblad, Comp. Phys. Comm. **71**, 15 (1992).

[33] G. Ingelman, A. Edin and J. Rathsman, Comp. Phys. Comm. **101**, 108 (1997).

[34] T. Sjöstrand, Comp. Phys. Comm. **39**, 347 (1986);
T. Sjöstrand and M. Bengtsson, Comp. Phys. Comm. **43**, 367 (1987);
T. Sjöstrand, Comp. Phys. Comm. **82**, 74 (1994).

[35] G. Marchesini et al., Comp. Phys. Comm. **67**, 465 (1992).

[36] M. Beckermann et al., Nucl. Inst. Meth. **A 479**, 334 (2002).

[37] D.P. Barber et al., Nucl. Inst. Meth. **A 329**, 79 (1993).

[38] ZEUS Coll., S. Chekanov et al., Phys. Rev. **D 67**, 012007 (2003).

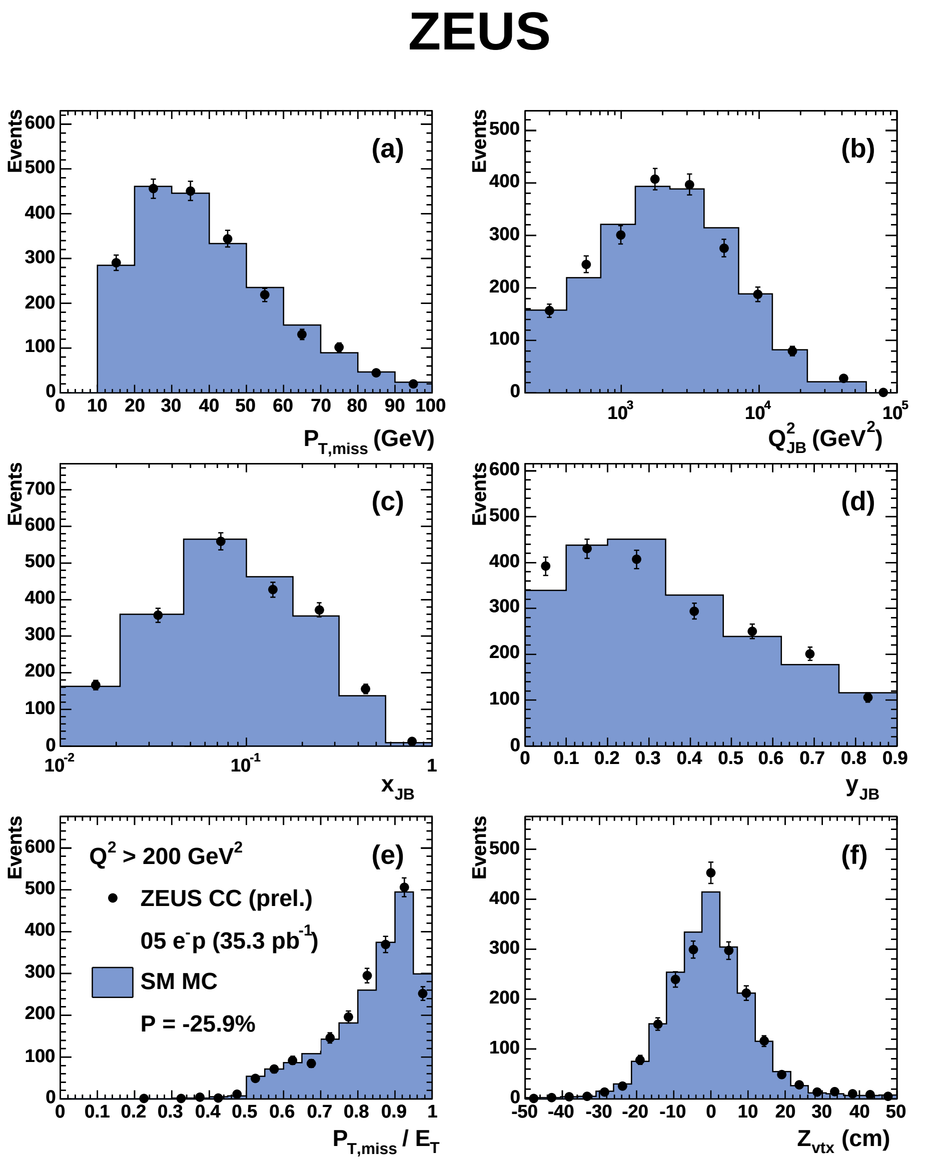

Figure 1: *Comparison of the final negative polarisation e^-p CC data sample with the expectations of the Monte Carlo simulation described in the text. The distributions of (a) missing transverse momentum, $P_{T,\rm miss}$, (b) $Q^2_{\rm JB}$, (c) $x_{\rm JB}$, (d) $y_{\rm JB}$, (e) $P_{T,\rm miss}/E_T$ and (f) the Z coordinate of the event vertex, Z_{vtx}, are shown.*

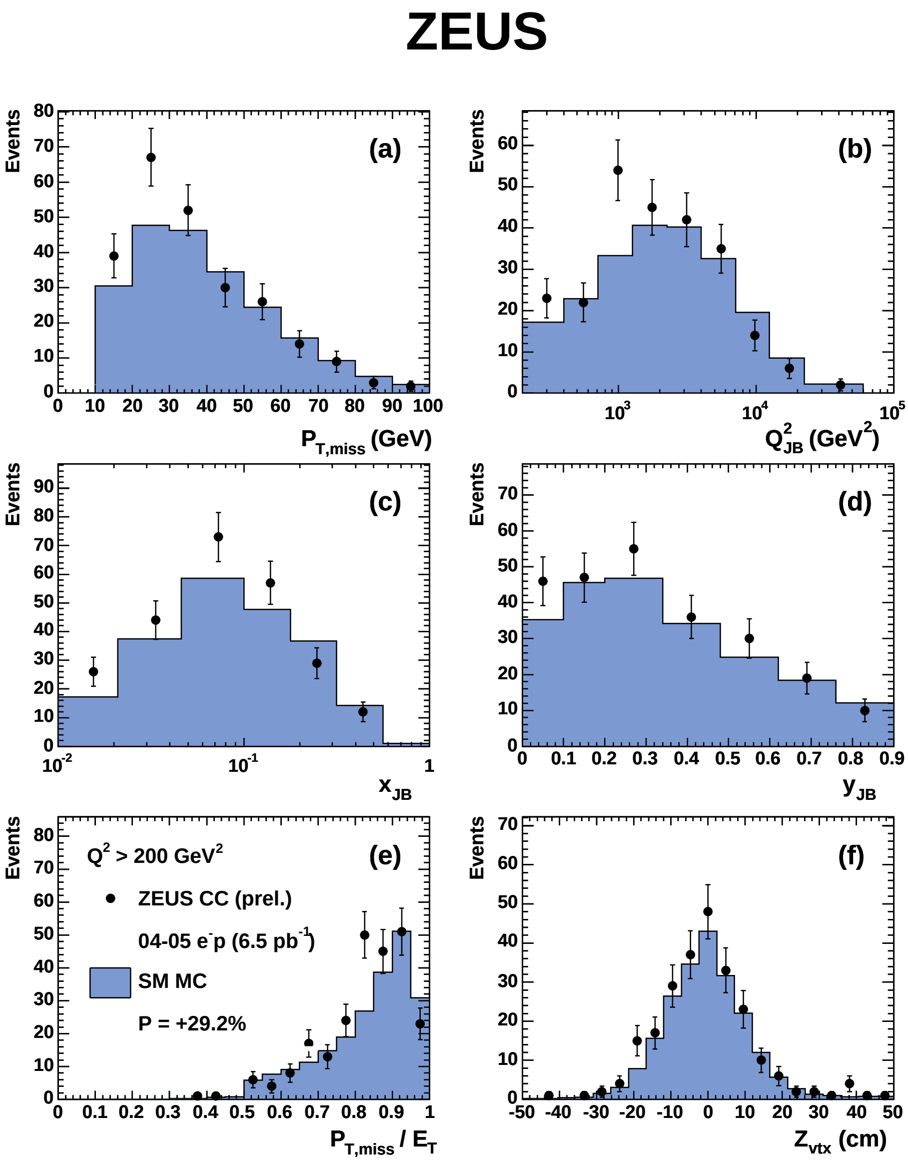

Figure 2: *Comparison of the final positive polarisation e^-p CC data sample with the expectations of the Monte Carlo simulation described in the text. The distributions of (a) missing transverse momentum, $P_{T,\mathrm{miss}}$, (b) Q^2_{JB}, (c) x_{JB}, (d) y_{JB}, (e) $P_{T,\mathrm{miss}}/E_T$ and (f) the Z coordinate of the event vertex, Z_{vtx}, are shown.*

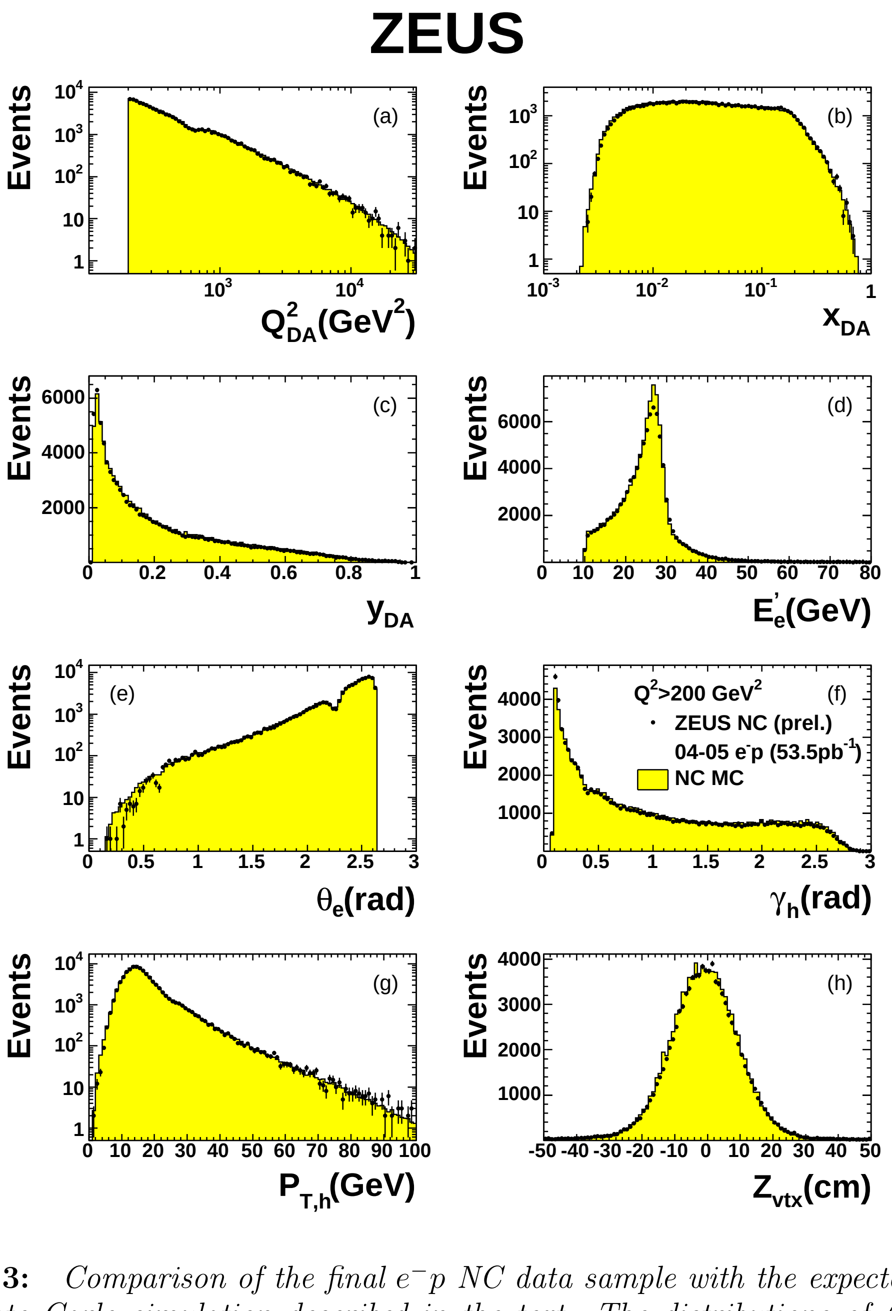

Figure 3: *Comparison of the final e^-p NC data sample with the expectations of the Monte Carlo simulation described in the text. The distributions of (a) $Q^2_{\rm DA}$, (b) $x_{\rm DA}$, (c) $y_{\rm DA}$, (d) the energy of the scattered electron, E'_e, (e) the angle of the scattered electron, θ_e, (f) the hadronic angle , γ_h, (g) the transverse momentum of the hadronic system, $P_{T,h}$, and (h) the Z coordinate of the event vertex, Z_{vtx}, are shown.*

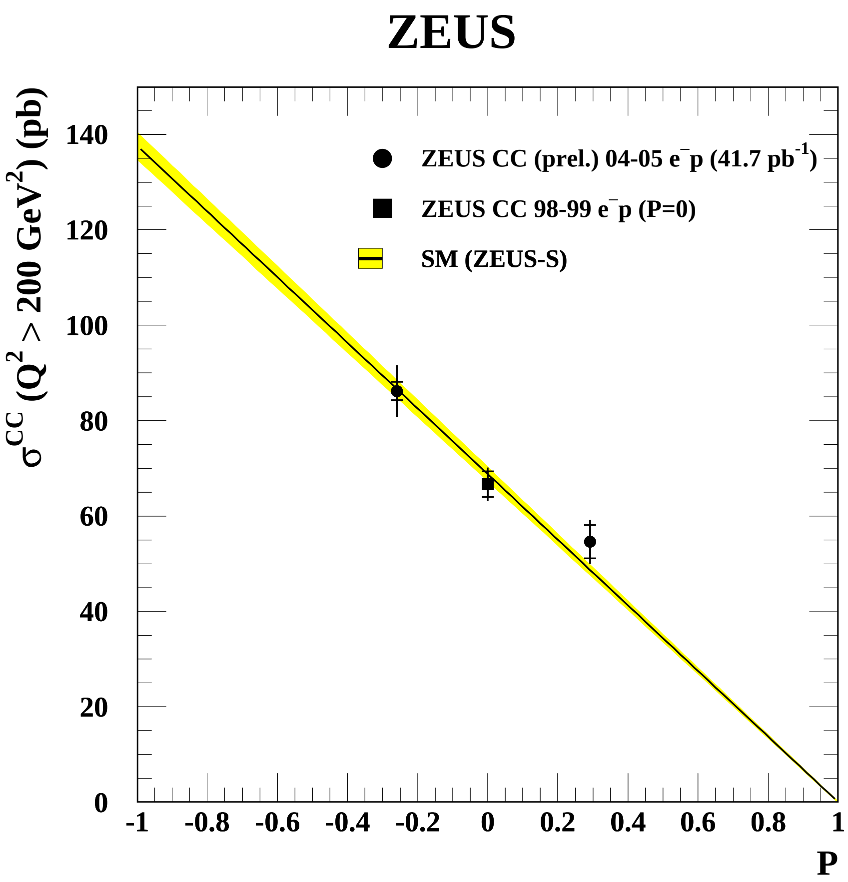

Figure 4: *The total cross section for e^-p CC DIS as a function of the longitudinal polarisation of the electron beam. The line shows the prediction of the SM evaluated using the ZEUS-S PDFs and the shaded band indicates the uncertainty on the cross section from the ZEUS-S fit.*

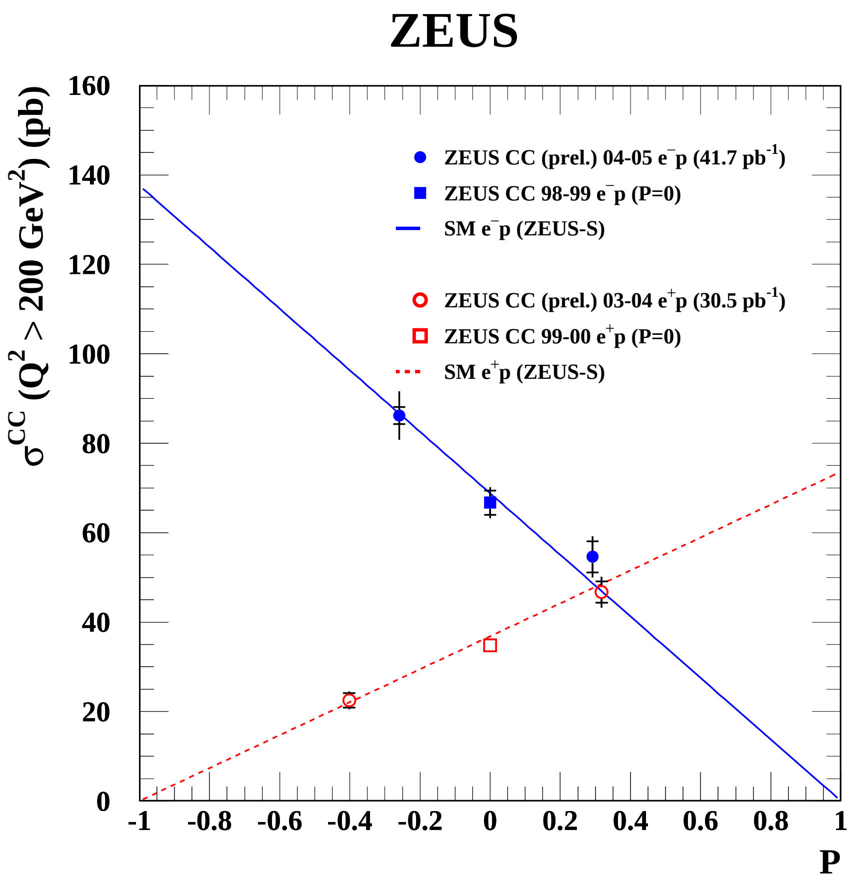

Figure 5: *The total cross sections for e^-p and e^+p CC DIS as a function of the longitudinal polarisation of the lepton beam. The lines shows the predictions of the SM evaluated using the ZEUS-S PDFs.*

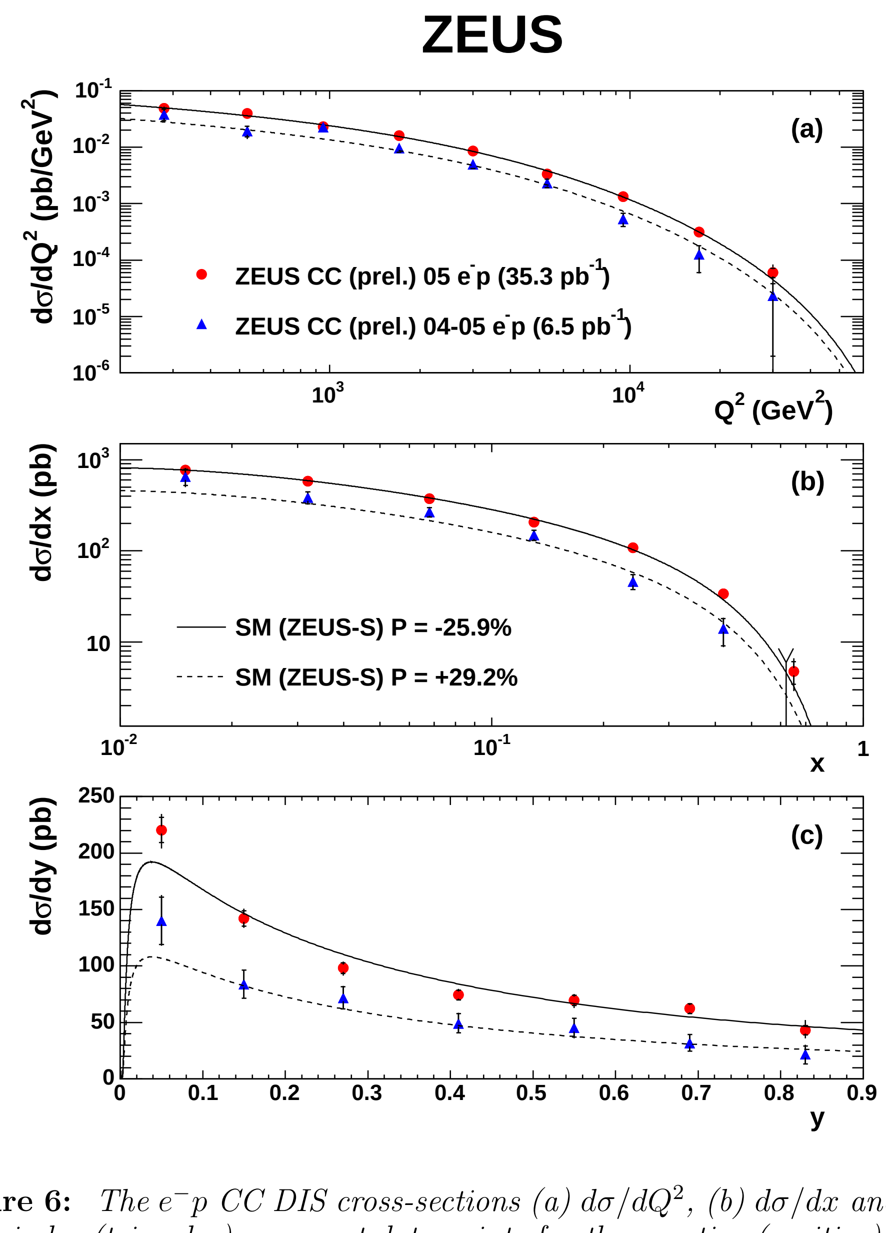

Figure 6: *The $e^{-}p$ CC DIS cross-sections (a) $d\sigma/dQ^2$, (b) $d\sigma/dx$ and (c) $d\sigma/dy$. The circles (triangles) represent data points for the negative (positive) polarisation measurements and the curves show the predictions of the SM evaluated using the ZEUS-S PDFs.*

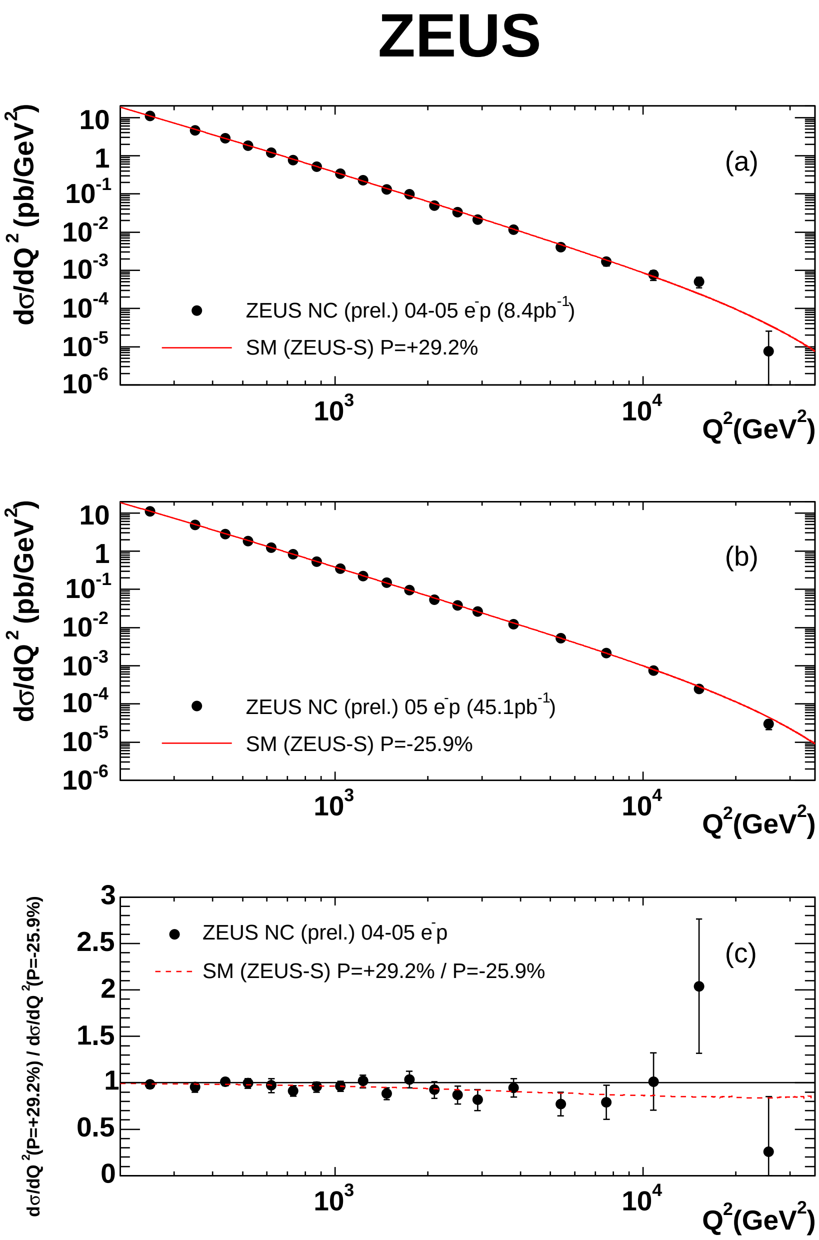

Figure 7: *The e^-p NC DIS cross-section $d\sigma/dQ^2$ for (a) positive polarisation data and (b) negative polarisation data and (c) the ratio of the two. The lines show the predictions of the SM evaluated using the ZEUS-S PDFs.*